Stable and Inert macrocyclic cobalt(II) and nickel(II) complexes with paraCEST response

Paulo Pérez-Lourido,[a] Enikő Madarasi,[b] Fanni Antal,[b] David Esteban-Gómez,[d] Gaoji Wang,[e] Goran Angelovski,[e,f] Carlos Platas-Iglesias,*[,d] Gyula Tircsó,[c] and Laura Valencia*[,a]

We report the synthesis of the macrocyclic ligands 3,9-PC2AM^{H} (2,2'-(3,6,9-triaza-1(2,6)-pyridinacyclodecaphane-3,9-diyl)diacetamide) and 3,9-PC2AM^{tBu} (2,2'-(3,6,9-triaza-1(2,6)-pyridinacyclodecaphane-3,9-diyl)bis(N-tert-butyl)acetamide) which contain a pyclen platform functionalized with acetamide or tert-butylacetamide pendant arms at positions 3 and 9 of the macrocyclic unit. The corresponding Co(II) and Ni(II) complexes were prepared, isolated and characterised as potential paramagnetic chemical exchange saturation transfer (paraCEST) agents. The X-ray structures of the Ni(II) complexes reveal six-coordination of the ligands to the metal ion. The Co(II) complex with 3,9-PC2AM^{tBu} shows a similar six-coordinate structure in the solid state, while the Co(II) complex with 3,9-PC2AM^{H} contains a seven-coordinate metal ion, seventh coordination being completed by the presence of an inner-sphere water molecule. The structure of the Co(II) complexes was investigated using ^{1}H NMR spectroscopy and computational methods. The complexes present a seven-coordinate structure in solution, as demonstrated by the analysis of the paramagnetic shifts using density functional theory. Ligand protonation constants and stability constants of the complexes with 3,9-PC2AM^{H} were determined using potentiometric titrations (I=0,15 M NaCl). The Co(II) complex was found to be more stable than the Ni(II) analogue (log K_{CoL} = 14.46(5) and log K_{NiL} = 13.15(3)). However, the Ni(II) and Co(II) complexes display similar rate constants characterizing the proton-assisted dissociation mechanism. The presence of highly shifted ^{1}H NMR signals due to the amide protons in slow exchange with bulk water results in sizeable CEST signals, which are observed at +67 and +15 ppm for the Co(II) complex with 3,9-PC2AM^{H} and +42 and +7 ppm for the Ni(II) analogue at 25 ºC .

Introduction

Chemical exchange saturation transfer (CEST) is an emerging mechanism that can be exploited to generate contrast in magnetic resonance imaging (MRI). Contrast agents based on the CEST effect contain a set of protons involved in slow-to-intermediate exchange with the surrounding water molecules. Saturation of the ^{1}H NMR signal of the exchangeable protons with a radiofrequency pulse may provoke the attenuation of the bulk water signal, thereby generating contrast.[1,2]

The CEST effect was first envisaged to be applied to endogenous protons,[3] and latter demonstrated using exogenous molecules such as amino acids and sugars.[4] Soon after, Sherry[5] and Aime[6] proposed the use of paramagnetic lanthanide complexes containing slowly exchanging water molecules or amide groups as CEST agents (paraCEST).[7,8,9] The paramagnetism of the metal ion may induce relatively large chemical shifts,[10] so that the signal of exchangeable protons is moved away from bulk water. This has some advantages with respect to diamagnetic CEST probes, as it minimizes the direct saturation of bulk water (radiofrequency spillover effect).[11] A second beneficial aspect is the possibility of shifting the CEST signal beyond the intrinsic signal of protons with restricted motion present in tissues, the so called tissue magnetization transfer window.[12] Finally, a large chemical shift difference between the two pools of protons allows meeting the slow-to-intermediate exchange condition with faster exchange rates. ParaCEST agents are particularly appealing to design probes with response to physiologically relevant parameters, such as pH or enzyme activity, using ratiometric approaches.[13]

Complexes of transition metal ions such as Fe(II),[14] Co(II),[15] Ni(II)[16] or Cu(II)[17] have been demonstrated to present interesting CEST properties, as they can induce large chemical shifts of exchangeable protons without provoking extreme line-broadening. Complexes of these metal ions may also present a better toxicity profile compared to the lanthanide ions, providing that they do not release the metal ion in vivo.[18] Furthermore, transition metal ions also have a rich redox chemistry that can be advantageous for the design of redox-responsive agents.[19,20]

The transition metal complexes explored so far as paraCEST agents contain amide, hydroxyl[21] or heterocyclic NH groups (i. e. pyrazole or imidazole)[22] as exchangeable protons.[23] Both macrocyclic and acyclic ligands were used for stable complexation of the paramagnetic metal, though detailed thermodynamic and kinetic studies are scarce.[24] Macrocyclic complexes are generally endowed with superior thermodynamic stability and kinetic inertness compared with similar acyclic ligands. The macrocyclic platforms most often employed are tetraazamacrocycles such as cyclam[25] and cyclen,[26,27] or the triaza macrocycle triazacyclononane (TACN).[28] Recently, the Co(II) and Ni(II) complexes of the pyclen-based ligand

[a] Departamento de Química Inorgánica, Facultad de Ciencias, Universidade de Vigo, As Lagoas, Marcosende, 36310 Pontevedra, Spain. E-mail: paulo@uvigo.es
[b] Doctoral School of Chemistry, Faculty of Science and Technology, University of Debrecen, H-4010, Debrecen, Egyetem tér 1, Hungary.
[c] Department of Physical Chemistry, Faculty of Science and Technology, University of Debrecen, H-4010, Debrecen, Egyetem tér 1, Hungary.
[d] Universidade da Coruña, Centro de Investigacións Científicas Avanzadas (CICA) and Departamento de Química, Facultade de Ciencias, 15071, A Coruña, Galicia, Spain. E-mail: carlos.platas.iglesias@udc.es
[e] MR Neuroimaging Agents, Max Planck Institute for Biological Cybernetics, 72076 Tübingen, Germany
[f] Laboratory of Molecular and Cellular Neuroimaging, International Center for Primate Brain Research (ICPBR), Center for Excellence in Brain Science and Intelligence Technology (CEBSIT), Chinese Academy of Sciences (CAS), 20031 Shanghai, PR China.

† Electronic supplementary information (ESI) available: Potentiometric and CEST experiments and details of the DFT study. CCDC 2108175-2108178. For ESI and crystallographic data in CIF or other electronic format
see DOI: 10.1039/x0xx00000x

PC3AM^{H} were also explored as paraCEST agents.[29] The rigidity that the pyridyl group introduces to the macrocyclic fragment may be beneficial to enhance the kinetic inertness of the complexes, as demonstrated recently for Mn(II).[30]

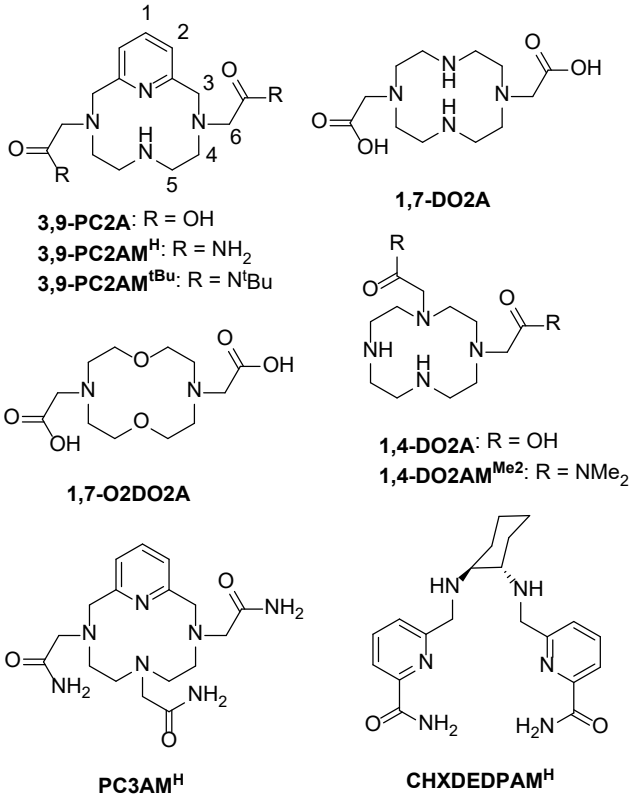

Scheme 1. Chemical structure of the ligands discussed in this work.

In this work, we present the Co(II) and Ni(II) complexes of the pyclen-based ligands 3,9-PC2AM^{H} and 3,9-PC2AM^{tBu} (Scheme 1). The 3,9-PC2AM^{tBu} ligand was prepared to assess whether secondary amide groups are well suited for paraCEST. Furthermore, the ^{1}H NMR signal of *t*Bu groups can be exploited to obtain paraSHIFT agents, providing that the signal is shifted from the diamagnetic window by the paramagnetism of the metal ion. We report a detailed assessment of the thermodynamic stability and dissociation kinetics of the complexes with 3,9-PC2AM^{H}, and the Co(II) and Ni(II) complexes with both 3,9-PC2AM^{H} and 3,9-PC2AM^{tBu} and their CEST properties.

Results and discussion

Synthesis. Both 3,9-PC2AM^{H} and 3,9-PC2AM^{tBu} where obtained by alkylation of the previously reported protected precursor N3-pyclen-Boc (**1**)[31] (Scheme 2) with 2-bromoacetamide or 2-bromo *tert*-butylamide[32] respectively, followed by removal of the Boc group using a 1:1 mixture of TFA and CH_2Cl_2 (see Experimental Section). The pure ligands were isolated with overall yields of 53% (3,9-PC2AM^{H}) and 59% (3,9-PC2Am^{tBu}) over the two steps. Reaction of the ligands with hydrated Co(II) or Ni(II) perchlorate salts in a 1:1 metal:ligand molar ratio afforded the corresponding complexes in good yields (70-82%).

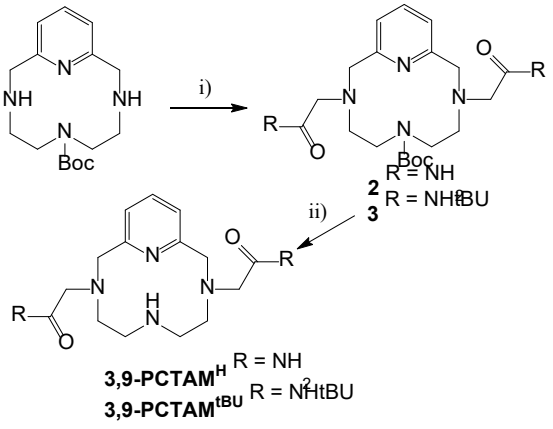

Scheme 2. Synthesis of the macrocyclic receptors 3,9-PC2AM^{H} and 3,9-PC2AM^{tBu}. Reagents and conditions: i) 2-bromo-acetamide (**2**) or 2-bromo-tertbutylamide (**3**), Na_2CO_3, CH_3CN, Δ; ii) TFA:CH_2Cl_2 (1:1), r. t.

X-ray structures. The structures of the Co(II) or Ni(II) complexes of PC2AM^{H} and PC2AM^{tBu} were determined using X-ray diffraction measurements (Figure 1). Crystals of the Co(II) complex with PC2AM^{H} contain in the asymmetric unit the $[Co(PC2AM^{H})(H_2O)]^{2+}$ cation, two PF_6^- anions and a water molecule involved in hydrogen bonds with the coordinated water molecule and the PF_6^- anions. The metal ion is directly coordinated to six donor atoms of the ligand comprising the four N atoms of the macrocyclic fragment and the two oxygen atoms of the acetamide groups. Seven-coordination is completed by the oxygen atom of a coordinated water molecule. The coordination polyhedron can be best described as a distorted pentagonal bipyramid, where O(1), O(2), N(1), N(2) and N(4) define the equatorial plane, and O(1W) and N(3) the axial positions. Shape measures confirm the pentagonal bipyramidal polyhedron, which displays a shape measure, S(A), lower than that of the capped trigonal prism (S(A) = 1.83 and 2.40, respectively).[33] However, the axial O(1W)-Co(1)-N(3) angle of 167.63(9)º presents a rather large deviation from the ideal value for a pentagonal bipyramid (180º). The Co(1)-O(1W) and Co(1)-N(3) bonds define angles with the donor atoms of the equatorial plane in the range 80.4-111.7º, which evidences large deviations from the ideal values of 90º. However, the bond angles defined by adjacent donor atoms of the equatorial plane (72.8-74.0º) are close to the value expected for a pentagonal bipyramid (72º). The axial donors O(1W) and N(3) provide the shortest distances of the metal coordination sphere (Table 1), as usually observed for pentagonal bipyramidal Co(II) complexes.[34,35]

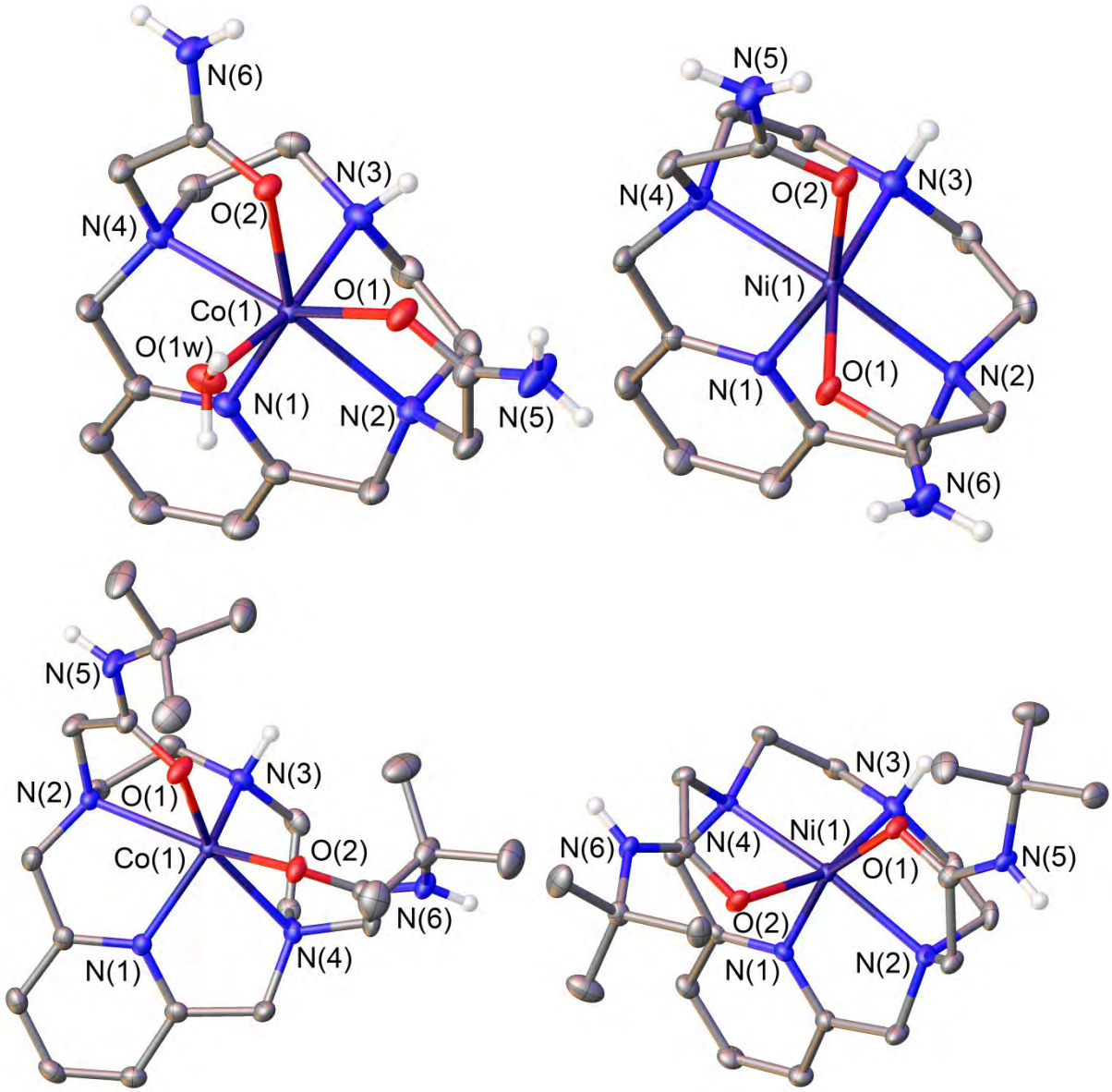

Figure 1. X-ray crystal structures of the cobalt(II) and nickel(II) complexes of 3,9-PC2AM^{H} (top) and 3,9-PC2AM^{tBu} (bottom). Hydrogen atoms bonded to carbon atoms are omitted for simplicity. Ellipsoids are at the 30% probability level.

Table 1. X-ray bond distances (Å) of the metal coordination environments in Co(II) and Ni(II) complexes of 3,9-PC2AM^{H} and 3,9-PC2AM^{tBu}.

	3,9-PC2AM^{H}	**3,9-PC2AM^{tBu}**		**3,9-PC2AM^{H}**	**3,9-PC2AM^{tBu}**
Co-N(1)	2.184(2)	2.084(5)	Ni-N(1)	1.9819(14)	1.9748(19)
Co-N(2)	2.359(2)	2.282(5)	Ni-N(2)	2.1351(14)	2.116(2)
Co-N(3)	2.113(2)	2.134(5)	Ni-N(3)	2.0583(15)	2.058(2)
Co-N(4)	2.290(2)	2.277(5)	Ni-N(4)	2.1260(14)	2.1284(19)
Co-O(1)	2.203(2)	2.044(4)	Ni-O(1)	2.0978(12)	2.0925(16)
Co-O(2)	2.201(2)	2.067(4)	Ni-O(2)	2.1191(12)	2.0724(16)
Co-O(1W)	2.104(2)				

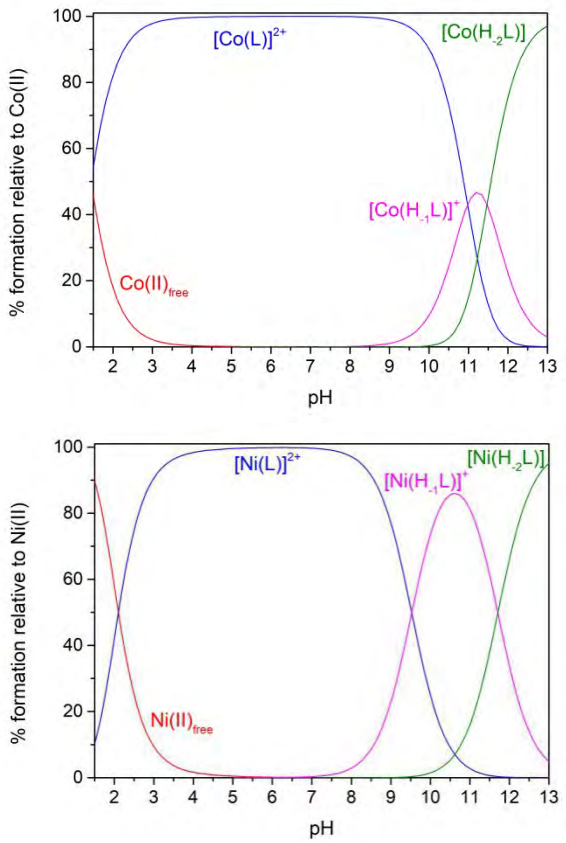

Figure 2. Species distribution curves of the M(II): 3,9-PC2AM^{H} systems (M = Co or Ni). $[M(II)]_{tot}$ = $[3,9\text{-PC2AM}^{H}]_{tot}$ = 10^{-3} M.

Crystals of the Co(II) complex with PC2AM^{tBu} contain two $[Co(PC2AM^{tBu})]^{2+}$ cations and four PF_6^- anions in the asymmetric unit (diffuse scattering associated with disordered water molecules was corrected). The Co(II) ions in both $[Co(PC2AM^{tBu})]^{2+}$ cations display a severely distorted trigonal prismatic six coordination environment [S(A) = 5.5], provided by the four nitrogen atoms of PC2AM^{tBu} and the two amide oxygen atoms.

The asymmetric units of the Ni(II) complexes with PC2AM^{H} and PC2AM^{tBu} contain the expected complex cations and two ClO_4^- or PF_6^- anions, respectively. The coordination environments of the metal ions in the two complexes are very similar. The metal ions are six-coordinate in a distorted octahedral fashion, being directly coordinated to the four nitrogen atoms of the macrocycle and the oxygen atoms of both amide groups. The *trans* angles N(1)-Ni(1)-O(2), N(3)-Ni(1)-O(1) and N(4)-Ni(1)-N(2) fall within the range 156.6-160.5º, reflecting important distortions of the octahedral coordination. Similarly, the *cis* angles also evidence important deviations from the ideal values of 90º (78.2-121.1º). The pyridine N atom N(1) provides the stronger bond with the Ni(II) ion (Table 1).

The macrocyclic pyclen moiety in the six-coordinate Co(II) and Ni(II) complexes adopts a rectangular [4242] conformation,[36] which is characterised by the presence of a mirror plane that bisects the macrocyclic fragment and the pyridyl group.[37] This macrocyclic conformation is often observed for complexes of transition metal ions containing pyclen fragments.[38] The conformation of the pyclen unit in the seven-coordinate $[Co(PC2AM^{H})(H_2O)]^{2+}$ cation is however [2334], with the two five-membered rings originated by coordination of the ethylenediamine groups adopting identical [(δδ) or (λλ)] conformations.[39] This likely facilitates the presence of a water molecule directly coordinated to the metal ion.

Ligand protonation constants and stability constants of the complexes. The protonation constants of the 3,9-PC2AM^{H} ligand were determined using potentiometric pH titrations in 0.15 M NaCl (Table 2). The ligand is characterised by one protonation constant corresponding to a fairly basic site ($\log K_1^{H}$ = 10.44(3)), and one corresponding to an acidic value ($\log K_2^{H}$ = 3.60(5)). These two protonation processes likely take place on the amine N atoms of the macrocycle.[31,40] The first protonation constant is considerably lower than that reported for 3,9-PC2A^{2-},[30] and effect that is commonly observed when acetate pendant arms are replaced by acetamide groups (i. e. 1,4-DO2A^{2-} and 1,4-DO2AM^{Me2}, Table 2).[41,42] The $\log K_1^{H}$ value of 3,9-PC2AM^{H} is similar to that determined for the amide derivative 1,4-DO2AM^{Me2}. However, 3,9-PC2AM^{H} is characterised by a rather low $\log K_2^{H}$ when compared to cyclen and 1,7-diaza-12-crown-6 derivatives such as 1,7-O2DO2A^{2-} (Table 2).[43] We attribute this effect to the rigidity introduced in the ligand scaffold by the presence of a pyridyl group, which results in a rather strong electrostatic repulsion between two protonated amine groups placed at a short distance. The protonation constants of PC3AM^{H} show a similar trend ($\log K_2^{H}$ = 4.10).[44]

The stability constants of the Co(II) and Ni(II) complexes with 3,9-PC2AM^{H} were also determined using potentiometric titrations (Table 3). The potentiometric titration curves evidenced two protonation processes that occur at rather high pH, which were characterised by the equilibrium constants shown in Eq (1):

$$K_{\mathrm{MH}_{-i}\mathrm{L}} = \frac{[\mathrm{MH}_i\mathrm{L}]}{[\mathrm{MH}_{i-1}\mathrm{L}][\mathrm{H}^+]} \qquad (1)$$

These processes can be assigned to the metal-induced deprotonation of amide groups.[45] The speciation diagrams (Fig 2) calculated from the equilibrium constants evidence that the deprotonation of amide groups in the Co(II) complex occurs above pH~9.0, while for the Ni(II) analogue deprotonation starts even at lower pH (> ~7.5). The higher acidity of the amide protons in the Ni(II) complex may be related to a stronger coordination of the amide group (Table 1), as evidenced in the X-ray structures described above, which likely polarizes the N-H amide bond.

Table 2. Protonation constants of PC2AM^{H} (T=25 ºC and *I*=0.15 M NaCl) and related ligands reported in the literature.

	PC2AM^{H}	**3,9-PC2A^{2-}** [a]	**1,4-DO2A^{2-}** [b]	**1,4-DO2AM^{Me2}** [c]	**1,7-DO2A^{2-}** [b]	**1,7-O2DO2A^{2-}** [d]
$\log K_1^{H}$	10.44(3)	12.25	11.44	10.14	11.69	9.53
$\log K_2^{H}$	3.60(5)	5.97	9.51	8.38	9.75	7.46
$\log K_3^{H}$		3.47	4.14		3.97	2.11

$\log K_4^H$		1.99	1.55		2.68	
$\Sigma \log K_2^H$	14.04	18.22	20.98	18.52	20.99	16.99

[a] Data in 0.15 M NaCl from Ref 30**¡Error! Marcador no definido.** [b] Data in 0.15 M NaCl from Ref 41. [c] Data in 0.1 M KCl from Ref 42. [d] Data in 0.1 M Me_4NNO_3 from Ref 43.

Table 3. Stability constants of the Co(II) and Ni(II) complexes formed with PC2AM^H (T=25 ºC and *I*=0.15 M NaCl) and related ligands reported in the literature.

	PC2AM^H	1,7-DO2A^{2-} [a]	1,7-O2DO2A$^-$ [b]
log K_{CoL}	14.46(5)	16.9	13.13
log K_{CoHL}	-	5.0	
log $K_{CoH\text{-}1L}$	10.98(7)		
log $K_{CoH\text{-}2L}$	11.47(6)		
log K_{NiL}	13.15(3)	>13.3	12.13
log $K_{NiH\text{-}1L}$	9.53(9)		
log $K_{NiH\text{-}2L}$	11.71(10)		

[a] Data from Ref 46. [b] Data from Ref 43a.

The stability constant determined for the Co(II) complex (logK_{CoL} = 14.46(5)) is ca. 1.5 log*K* units higher than that determined for the Ni(II) analogue (logK_{NiL} = 13.15(3)), a situation that is also observed for the complexes with 1,7-DO2A^{2-} and 1,7-O2DO2A^{2-}.[43,46] This trend is in contradiction with the Irving-Williams series,[47] which predicts higher stability for Ni(II) complexes compared to Co(II) analogues. However, the Irving-Williams trend holds strictly only for high-spin octahedral complexes. The X-ray structures described above evidence that Co(II) forms a seven-coordinate complex with 3,9-PC2AM^H, while the Ni(II) analogue displays a six-coordinate environment. A seven-coordinate Co(II) centre was also observed for the [Co(1,7-O2DO2AM^H)]$^{2+}$ complex both in the solid state and in solution, thanks to the presence of an inner-sphere water molecule.[48] It has been shown that pentagonal bipyramidal coordination is particularly unfavourable for Ni(II) due to the Jahn-Teller effect.[49,50] As a result, complexes with ligands pre-organised for pentagonal bipyramidal coordination, as 1,7-diaza-12-crown-4 derivatives, display either very distorted seven-coordinate coordination environments or even octahedral coordination. In the latter case, one of the donor atoms of the pentadentate macrocyclic fragment remains uncoordinated. Thus, we attribute the stability trend of 3,9-PC2AM^H complexes Co(II) > Ni(II) to the ability of the ligand to form a particularly stable seven-coordinate Co(II) complex.

Dissociation kinetics. Kinetic inertness is a key property that should be considered when designing metal complexes for medical applications. This issue is particularly critical for MRI agents, due to the high doses of the contrast agent that are generally injected. The dissociation kinetics of Gd(III)-based MRI agents have been studied in great detail,[51] while some studies have been also reported for Mn(II) contrast agent candidates.[41] However, the studies of the dissociation kinetics of paraCEST agents based on transition metal complexes are scarce. In most cases, the lack of dissociation in a competitive medium such as serum is considered as a good indication of inertness.[28] However, these studies do not provide information on the role of the different mechanisms leading to complex dissociation and their contributions.

The dissociations of the Co(II) and Ni(II) complexes of 3,9-PC2AM^H were evaluated under acidic conditions in the H$^+$ concentration range 0.1 – 1.0 M (*I* = 1 M NaCl, 25 ºC). The reaction was monitored by following the changes in the UV absorption spectra at 230 nm. The large excess of H$^+$ ensures pseudo-first order conditions, so that the observed rate constants can be expressed as in Eq (2):

$$-\frac{d[\mathrm{ML}]t}{dt} = k_{obs}[\mathrm{ML}]_t \qquad (2)$$

The values of k_{obs} can be therefore obtained by fitting the absorption data to Eq (3), where A_t, A_o and A_e are the absorptions of the complex at time *t*, *t* = 0 and at equilibrium, respectively.

$$A_t = A_e + (A_0 - A_e)e^{-k_{obs}t} \qquad (3)$$

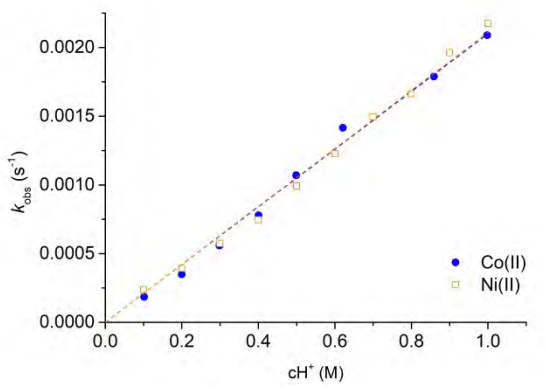

Figure 3. Dissociation rates (k_{obs}) for the [Co(PC2AM^H)]$^{2+}$ and [Ni(PC2AM^H)]$^{2+}$ complexes as a function of proton concentration. The straight lines correspond to the linear least-squares fit of the data.

The plots of the k_{obs} values versus H$^+$ concentration provide straight lines (Figure 3), which indicates that the rate constants present first-order dependency with proton concentration. Thus, the kinetic data were fitted to Eq (4), where k_0 and k_1 are the rate constants characterising the spontaneous and proton-assisted dissociation, respectively.

$$k_{obs} = k_0 + k_1[\mathrm{H}^+] \qquad (4)$$

The fit of the data provided negligible values of k_0, which indicates that the spontaneous dissociation does not play any role under the experimental conditions used for the kinetic experiments. The values of k_1 obtained for the Co(II) and Ni(II) complexes are very similar, with values of (2.10±0.04)×10^{-3} and (2.11±0.03)×10^{-3} M^{-1} s^{-1}, respectively. Detailed kinetic studies for Co(II) and Ni(II) complexes are relatively rare, thus it is difficult to make direct comparisons. The Ni(II) chelates formed with CHXDEDPA and its primary amide derivative CHXDEDPAM^H were studied previously.[24] These Ni(II) complexes were found to dissociate by a slightly different mechanism, as the plots of the k_d values as a function of H$^+$ concentration showed a quadratic dependence, suggesting that the dissociation might take place through a proton-assisted pathway involving mono- and di-protonated species characterized by rate constants k_1 (M^{-1}s^{-1}) and k_2

($M^{-2}s^{-1}$), whereas in our case linear dependence was observed (i.e. only the value of k_1 can be calculated). Furthermore, for the di-picolyl(amide) derivative it was not possible to determine the k_1 rate constant, yet the data show that the given chelate dissociates with a slower rate, which is in agreement with the trend observed for the Mn(II) and Gd(III) complexes of ligands obtained as a result of replacement of acetate pendants by amides.[42,52]

By comparing the k_1 values obtained for Ni(CHXDEDPA) (6.1×10^{-4} $M^{-1}s^{-1}$) and $[Ni(3,9\text{-}PC2AM^{H})]^{2+}$, it can be concluded that the Ni(II) complex formed by the chelator derived from the rigid *trans*-cyclohexanediamine platform possessing rigid picolinate moieties is more inert (k_1 is half the value of that of $[Ni(3,9\text{-}PC2AM^{H})]^{2+}$). Another possibility to assess the reactivity of these complexes is to compare the pseudo-first-order rate constants (k_d) determined under similar conditions. The k_d constants determined using 1.0 M HCl were found to be 9.05×10^{-4}, 1.69×10^{-4} and 2.09×10^{-3} s^{-1} for [Ni(CHXDEDPA)], $[Ni(CHXDEDPAM^{H})]^{2+}$ and $[Ni(3,9\text{-}PC2AM^{H})]^{2+}$, respectively. These data confirm that Ni(CHXDEDPA) and $Ni(3,9\text{-}PC2AM^{H})^{2+}$ complexes possess similar kinetic reactivity, while $[Ni(CHXDEDPAM^{H})]^{2+}$ is considerably more inert towards acid assisted dissociation. The kinetic data also indicate that Co(II) and Ni(II) complexes are in general more inert than Mn(II) chelates, as for the latter the lowest k_1 value reported in literature is $1.6\text{-}2.2\times10^{-3}$ M^{-1} s^{-1}, which was observed for a Mn(II) complex formed with bispidine (3,7-diazabicyclo[3.3.1]nonane) derivative.[53] On the other hand, the rates of acid-assisted dissociation of $[Co(3,9\text{-}PC2AM^{H})(H_2O)]^{2+}$ and $[Ni(3,9\text{-}PC2AM^{H})]^{2+}$ complexes are similar to that of [Gd(HP-DO3A)], which is a Gd(III)-based MRI contrast agent marketed under the trade name Prohance®.[54]

Solution structure. The ^{1}H NMR spectra of the Ni(II) complexes are poorly resolved and resulted to be rather uninformative. However, ^{1}H NMR spectrum of the $[Co(PC2AM^{H})(H_2O)]^{2+}$ complex recorded in D_2O solution is well resolved (Figure 4). It shows ten paramagnetically shifted signals in the range ~18 to 133 ppm. This is consistent with an effective C_s symmetry in solution, where the mirror plane bisects the macrocyclic fragment and the pyridyl ring. The signals due to the pyridyl protons H1 and H2 can be easily identified at 19.2 and 57.1 ppm, respectively, because of their sharpness and relative integrations (see Scheme 1 for labelling). The macrocyclic [2334] conformation observed in the solid state does not result in a C_s symmetry, which is likely achieved by a change in the conformation of the five-membered chelate rings involving the ethylenediamine units: (δδ)↔(λλ). The linewidths of the ^{1}H NMR signals support this hypothesis, as two relatively sharp signals are observed at 132.9 and 108.8 ppm. These resonances can be attributed to the equatorial CH_2 protons of the acetamide pendant arms (H6) and those linked to the pyridyl ring (H3). A full analysis of the spectrum was achieved by performing linewidth analysis and calculation of the paramagnetic shifts.

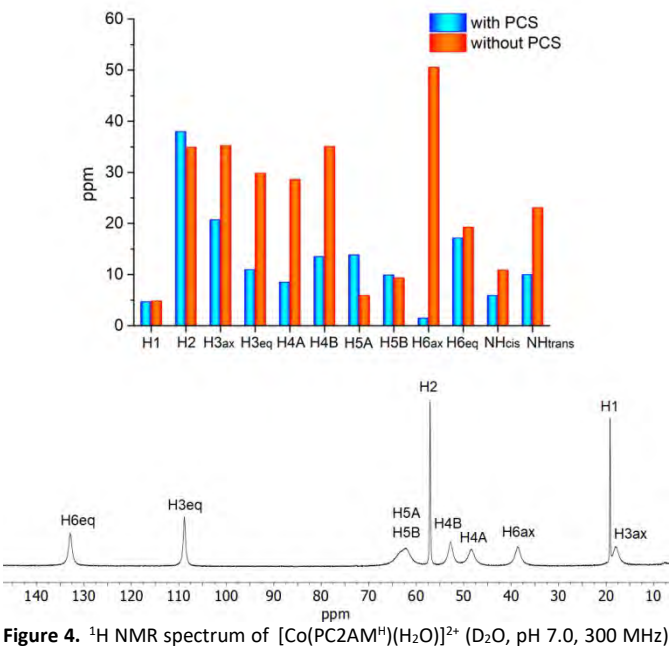

Figure 4. ^{1}H NMR spectrum of $[Co(PC2AM^{H})(H_2O)]^{2+}$ (D_2O, pH 7.0, 300 MHz) and absolute deviations of the calculated versus experimental shifts with and without including pseudocontact shifts (PCS). See Scheme 1 for labelling.

The paramagnetic shifts of nuclei in the vicinity of Co(II) are often dominated by the contact contribution, which arises from a through-bond transmission of unpaired spin density following spin delocalization and spin polarization mechanisms.[55,56] However, contact contributions drop quickly on increasing the number of chemical bonds separating the observed nucleus and the paramagnetic centre. Indeed, it has been shown that the ^{1}H NMR chemical shifts of remote nuclei with respect to the Co(II) centre show sizeable pseudocontact shifts.[57] The nuclear shielding (σ) in a paramagnetic Co(II) complex can be expressed as a sum of the diamagnetic (σ^{dia}) and paramagnetic (σ^{para}) contributions:

$$\sigma = \sigma^{\mathrm{dia}} + \sigma^{\mathrm{para}} \quad (5)$$

Recent theoretical investigations showed that the paramagnetic shift can be expressed as in Eq (6), assuming that spin-orbit coupling can be considered as a small perturbation, which leads to the spin Hamiltonian defined as Eq (7).[58,59]

$$\sigma^{para} = -\frac{\beta_e S(S+1)}{g_N \beta_N 3kT}\mathbf{gZA} \quad (6)$$

$$H = \mathbf{S}\cdot\mathbf{D}\cdot\mathbf{S} + \beta_e \mathbf{B}\cdot\mathbf{g}\cdot\mathbf{S} + \mathbf{S}\cdot\mathbf{A}\cdot\mathbf{I} \quad (7)$$

In these equations, **g** and **A** represent the g- and A-tensors, **Z** is a 3×3 matrix that depends on the zero field splitting (ZFS) and temperature and other symbols have their usual meaning.

The ^{1}H chemical shifts of the $[Co(PC2AM^{H})(H_2O)]^{2+}$ complex were estimated using Eqs (5)-(6), using the A-tensors obtained with DFT calculations. The X-ray structure described above was used in these calculations, after optimizing the positions of the H atoms only (see computational details). The calculated A-tensors and isotropic hyperfine coupling constants A^{iso} are highly sensitive to the choice of the functional and the amount of Hartree−Fock exchange.[56] We thus performed a set of calculations of the A-tensors of ^{1}H nuclei employing different functionals, and estimated the paramagnetic shifts using Eq (6) and neglecting the contributions of ZFS and *g*-

tensors. These tests reflected that the paramagnetic shifts are indeed very sensitive to the amount of HF exchange, with larger amounts of HF exchange generally leading to smaller paramagnetic shifts (Table S1, ESI†). The BH&HLYP functional (50% HF exchange) was found to provide the best agreement with the experimental data, and was thus selected for further analysis. The inclusion of g- and D-tensors obtained with DFT did not improve significantly the agreement with the experimental data. We note that the calculation of these parameters using DFT is not a trivial task, the results being strongly dependent on the functional used. Having this in mind, we sought to use the A-tensors obtained with DFT to estimate the contact contributions (σ^c) with Eq (6), and describe the contribution to the paramagnetic chemical shift arising from the anisotropic distribution of the unpaired electrons using the classical expression of the pseudocontact shift derived from semiempirical theory:[60,61]

$$\sigma^{pc} = -\frac{1}{2N_A}\left[(\chi_{zz} - \chi_{av})\left(\frac{3z^2-r^2}{r^5}\right) + (\chi_{xx} - \chi_{yy})\left(\frac{x^2-y^2}{r^5}\right)\right] \quad (8)$$

$$r = \sqrt{x^2 + y^2 + z^2} \quad (9)$$

In these expressions x, y and z are the Cartesian coordinates of the observed nuclei with the paramagnetic metal ion placed at the origin and χ_{xx}, χ_{yy} and χ_{zz} are the components of the diagonal magnetic susceptibility tensor. The diamagnetic contribution (σ^{dia}) was estimated with DFT using the well-established GIAO method. Thus, the calculated chemical shift δ^{cal} can be expressed as in Eq (10), where σ^{ref} represents the shielding constant of tetramethylsilane.

$$\delta^{\mathrm{cal}} = \sigma^{\mathrm{ref}} - \sigma^{\mathrm{dia}} - \sigma^{\mathrm{c}} - \sigma^{\mathrm{pc}}) \quad (10)$$

The results of the analysis (Table 4) show that the experimental shifts are predicted to a reasonable accuracy for most protons, with the exception of H2 and particularly H3ax, which present somewhat large deviations. The H2 protons present a rather large paramagnetic shift in spite of being 4 bonds away the paramagnetic centre; hence, calculations clearly underestimate its paramagnetic shift. We note that the diamagnetic shifts (δ^{dia} = σ^{ref}-σ^{dia}) are very reasonable considering the nature of the different nuclei. The chemical shifts of equatorial protons present large contact contributions, as observed previously for paramagnetic lanthanide complexes.[62] Due to the different conformations of the two chelates containing protons H4 and H5, each resonance is actually the average of the chemical shift of an axial and an equatorial proton. Most protons present significant contact and pseudocontact contributions, the latter being dominant for H4A, H4B and H6ax.

Table 4. Chemical shifts (ppm) observed for $[Co(PC2AM^H)(H_2O)]^{2+}$, values calculated using Eqs (5)-(10) and the corresponding diamagnetic, contact and pseudocontact contributions.

	σ^{ref}-σ^{dia}	σ^{c}	σ^{pc}	δ^{cal}	δ^{exp}
H1	8.52	-15.48	9.49	14.51	19.17
H2	7.79	-14.38	3.02	19.14	57.09
H3ax	4.37	21.60	-14.53	-2.70	18.00
H3eq	4.39	-74.63	-18.84	97.85	108.8
H4A	2.22	-7.79	-20.12	30.13	38.62
H4B	2.36	-10.93	-21.56	34.85	48.36
H5A	2.20	-54.18	7.90	48.48	62.30
H5B	1.59	-70.54	19.25	52.88	62.77
H6ax	3.65	1.46	-49.08	51.27	52.75
H6eq	3.79	-110.8	-36.41	150.0	132.9
NH_{cis} [a]	6.29	-2.52	-4.97	13.78	19.70
NH_{trans}[a]	6.51	-42.33	-13.07	61.71	71.70

[a] Amide protons in cis and trans with respect to the amide O atom. Experimental shifts estimated from CEST spectra.

The agreement between the experimental and calculated shifts improves considerably upon inclusion of the pseudocontact term (Figure 4). The values of the axial and rhombic components of the susceptibility tensor obtained from the fit of the data are χ_{zz}-χ_{av} = 0.02 cm^3 K mol^{-1} and χ_{zz}-χ_{av} = 0.97 cm^3 K mol^{-1}, which shows that the pseudocontact contribution is largely dominated by the rhombic term.

The relatively good agreement between the experimental and calculated ^{1}H NMR shifts of $[Co(PC2AM^H)(H_2O)]^{2+}$ confirms that the structure observed in the solid state is essentially maintained in solution. Furthermore, the ^{1}H NMR spectrum of the complex with the $PC2AM^{tBu}$ shows very similar chemical shifts (Figure S15, ESI†), which suggests that a water molecule coordinates to the metal ion in solution, resulting in similar structures for the two complexes. This is in contrast to the structures observed in the solid state, which evidence different coordination numbers (see above).

CEST spectra. The crystal structure studies showed the presence of exchangeable amide protons, suggesting possible CEST features of the investigated complexes. The CEST effects were analysed by recording a series of z-spectra on the $PC2AM^H$-based Co(II)/Ni(II) complexes at 25 °C, and by applying saturation powers of 2.5, 5, 10, 15, 20, 25 and 30 μT, with a duration of the radio frequency pulses of 2s. The shapes and intensities of CEST signals change with different saturation powers (Figure S16 and S17, ESI†). At 15 μT, the chemical shifts were +67 ppm with the CEST effect of ~10% and +15 ppm (CEST effect of ~5%) for the Co(II) complex, while for Ni(II) complex the signals are observed at +42 ppm (CEST effect of ~5%) and +7 ppm (CEST effect of ~3%, Figure 5). The two CEST signals were assigned to the NHcis and NHtrans amide protons on the basis of the DFT calculations presented in the previous section, with amide protons in *trans* position with respect to the amide oxygen atom being responsible for the most shifted signal (Table 4).

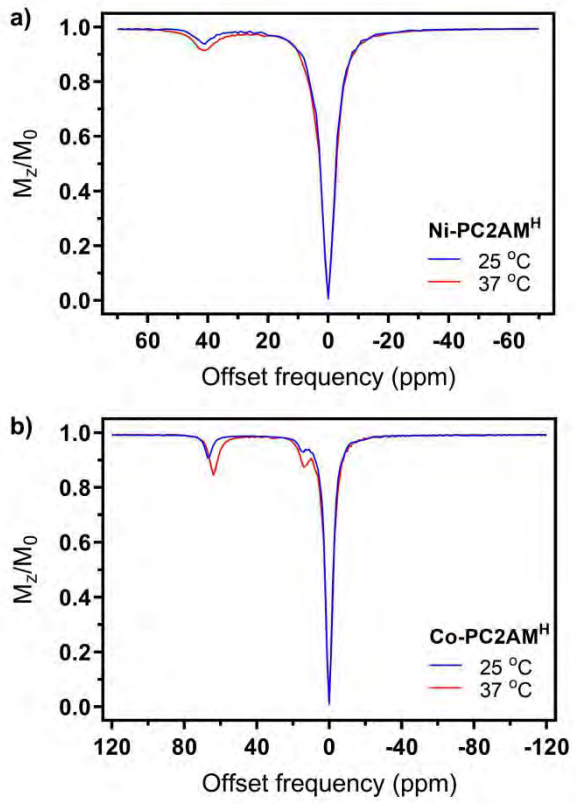

Figure 5. CEST spectra of a) 15 mM $[Ni(PC2AM^H)]^{2+}$ and b) 20 mM $[Co(PC2AM^H)(H_2O)]^{2+}$ (50 mM HEPES, pH 7.4 300 MHz) at different temperatures with a saturation time of 2 s and saturation power of B_1= 15 μT.

Temperature influences the exchange rate of amide protons; thus higher temperature results in faster proton exchange and stronger intensity of CEST signal within the reasonable temperature range. Concurrently, stronger CEST effects are observed when increasing the temperature from 25 to 37 ºC, with the position of the amide signal shifting from +67 to +64 ppm for Co(II) complex and remaining almost unaffected at +42 ppm for the Ni(II) derivative. The corresponding exchange rates (k_{ex}) were assessed using the qCEST method based on the Bloch–McConnell (BM) equations. The obtained results provided k_{ex} values of 1173 Hz (+67 ppm) and 141 Hz (+15 ppm) for the Co(II) complex and 3519 Hz (+42 ppm) and 1285 Hz (+7 ppm) for Ni(II) complex at 25 ºC. At the higher temperature (37 ºC), the corresponding k_{ex} values accelerated to 2951 and 1271 Hz for the Co(II) complex and 5994 and 1665 Hz for the Ni(II) complex, for the higher and lower shifting CEST effects, respectively. These k_{ex} values fall into the suitable range of values that are optimal for obtaining the maximal CEST effect MRI scanners used for the preclinical studies.[63] These k_{ex} values also show that NH_{trans} protons are characterised by faster water exchange rates than the NH_{cis} ones, as observed previously for di-picolyl(amide) Ni(II) derivatives.[24] The exchange rates determined at 37 ºC compare well with those reported for the Ni(II) and Co(II) complexes with $PC3AM^H$.[29] We notice however that lower amide exchange rates were determined at the same temperature for different Ni(II) and Co(II) complexes containing amide groups, typically 300-900 Hz.[64] This suggests that the exchange rates of amide protons are rather sensitive to the nature of the complex, with an increased acidity of amide protons leading to faster exchange rates.[65] Finally, no visible CEST signal was detected for $PC2AM^{tBu}$-based Co(II)/Ni(II) complexes, likely due to slow exchange of amide protons in the presence of electron donating *t*Bu groups.

Conclusions

We have reported a detailed characterization of Co(II) and Ni(II) complexes with pyclen-based ligands containing amide pendant arms. These complexes were conceived to provide CEST effect upon applying a radiofrequency pulse to the amide proton signals. The complexes present a rather high stability in aqueous solution, with the Co(II) complexes showing a higher stability. The analysis of the paramagnetic ^{1}H NMR shifts of the $[Co(PC2AM^H)(H_2O)]^{2+}$ complex suggests that the seven-coordinate structure observed in the solid state is maintained in solution. The $[Co(3,9\text{-}PC2AM^H)(H_2O)]^{2+}$ and $[Ni(3,9\text{-}PC2AM^H)]^{2+}$ complexes possess similar dissociation kinetic properties to that of [Gd(HP-DO3A)], a commercially available CA based on a macrocyclic ligand. Therefore, one can assume that dissociation kinetic data determined for these complexes should not be an obstacle for further development. CEST properties of both $PC2AM^H$-based complexes indicate that CEST effects are moderate, mainly due to the low number of exchangeable protons per molecule, albeit their exchange values are in the appropriate range. Thus this study provides valuable insights in the structural parameters that lead to the formation of stable transition metal complexes with paramagnetic features that are suitable for the development of new class of potential MRI agents.

Experimental Section

Measurements. Infra-red (IR) spectra were recorded on a Bruker VECTOR 22 spectrometer. ESI experiments were performed on an microTOF(focus) mass spectrometer (Bruker Daltonics, Bremen, Germany). Ions were generated using an ApolloII (ESI) source and ionization was achieved by electrospray. ^{1}H NMR spectra were recorded in D_2O solutions, on a Bruker ARX400 NMR spectrometer.

Materials. All commercially available chemicals were purchased with the highest purity and used without further purification. Compounds **1**[66] and 2-bromo-tertbutylamide[67] were synthesized following the published methods. Hydrated cobalt(II) and nickel(II) perchlorates were obtained from Aldrich. Solvents were of reagent grade and purified by the usual methods.

Synthesis of *tert*-butyl 3,9-bis(2-amino-2-oxoethyl)-3,6,9-triaza-1(2,6)-pyridinacyclodecaphane-6-carboxylate (2). A solution of 2-bromoacetamide (0.78 g, 5.64 mmol) in dry acetonitrile (20 mL) was added dropwise to a suspension of **1** (0.87 g, 2.82 mmol) and Na_2CO_3 (1.20 g 11.3 mmol) in the same solvent (80 mL). The reaction mixture was refluxed overnight and then allowed to cool to room temperature. The mixture was filtered off and the solution was concentrated under vacuum. The residue was taken up in 30 mL of chloroform and extracted with water (3 x 20 mL). The organic layer was dried over sodium sulphate and concentrated under vacuum to afford compound **2** as a pale yellow solid. Yield: 0.96 g (81%). $C_{20}H_{32}N_6O_4$ (420.51): calcd. C 57.1, H 7.7, N 20.0; found C 57.0, H 7.8, N 19.8. IR (ATR, cm^{-1}): 1586 (s), 1454 (s) [ν(C=C) and $\nu(C=N)_{py}$], 1633

(s), 1693 (s) [ν(C=O)], 3376 (m) [ν(NH)]. MS (ESI-MS, *m/z,* found (calculated)): 421 (421) [**2**+H]$^+$. ^{1}H NMR ($CDCl_3$) δ: 7.68 (t, 1H), 7.16 (d, 2H, ^3J = 7.7 Hz), 3.84 (s, 4H), 3.31 (s, 4H), 3.26 (b, 4H), 2.95-2.61 (m, 4H), 1.36 (s, 9H).

Synthesis of *tert*-butyl 3,9-bis(2-(*tert*-butylamino-2-oxoethyl)-3,6,9-triaza-1(2,6)-pyridinacyclodecaphane-6-carboxylate (3). A solution of 2-bromo-tertbutylamide (0.96 g, 4.90 mmol) in dry acetonitrile (20 mL) was added dropwise to a suspension of **1** (0.75 g, 2.45 mmol) and Na_2CO_3 (1.06 g 10 mmol) in the same solvent (80 mL). The reaction mixture was refluxed overnight and then allowed to cool to room temperature. The mixture was filtered off and the solution was concentrated under vacuum. The residue was taken up in 30 mL of chloroform and extracted with water (3 x 20 mL). The organic layer was dried over sodium sulphate and concentrated under vacuum to afford compound 3 as a pale yellow solid. Yield: 1.09 g (84%). $C_{28}H_{48}N_6O_4$ (532.7): calcd. C 63.1, H 9.1, N 15.8; found C 63.0, H 9.9, N 15.8. IR (ATR, cm^{-1}): 1515 (s), 1454 (s) [ν(C=C) and ν(C=N)$_{py}$], 1664 (s) [ν(C=O)], 3275 (m) [ν(NH)]. MS (ESI-MS, *m/z,* found (calculated)): 533 (533) [**3**+H]$^+$. ^{1}H NMR ($CDCl_3$) δ: 7.71 (t, 1H), 7.16 (d, 2H, ^3J = 7.7 Hz), 3.83-3.77 (m, 4H), 3.31 (m, 4H), 3.17 (s, 4H), 2.83-2.58 (m, 4H), 1.39 (s, 18H), 1.37 (s, 9H).

Synthesis of 2,2'-(3,6,9-triaza-1(2,6)-pyridinacyclodecaphane-3,9-diyl)diacetamide (3,9-PC2AM^{H}) and 2,2'-(3,6,9-triaza-1(2,6)-pyridinacyclodecaphane-3,9-diyl)bis(N-tert-butyl)acetamide (3,9-PC2AM^{tBu}). Compound **2** (for **3,9-PC2AM^{H}**) or **3** (for **3,9-PC2AM^{tBu}**) (0.50 mmol) was stirred for 24 hours in 12 mL of a mixture of CH_2Cl_2/trifluoroacetic acid (TFA) in a 1:1 ratio. After concentrating the mixture under vacuum, the residue was dissolved in 40 mL of water. A saturated NaOH solution was added until basic pH and extracted with dichloromethane (4x30 mL). Finally, the organic layer was dried over sodium sulphate and concentrated under vacuum to afford **3,9-PC2AM^{H}** or **3,9-PC2AM^{tBu}** as pale yellow solids.

3,9-PC2AM^{H}: Yield: 0.11 g (65%). $C_{15}H_{26}N_6O_3$ (338.4): calcd. C 53.2, H 7.7, N 24.8; found C 53.0, H 7.6, N 24.8. IR (ATR, cm^{-1}): 1596 (s), 1452 (s) [ν(C=C) and ν(C=N)$_{py}$], 1633 (s), 1651 (s) [ν(C=O)], 3262 (m) [ν(NH)]. MS (ESI-MS, *m/z,* found (calculated)): 321 (321) [**3,9-**PC2AM^{H} +H]$^+$. ^{1}H NMR ($CDCl_3$) δ: 7.61 (t, 1H), 7.13 (d, 2H, ^3J = 7.7 Hz), 3.89 (s, 4H), 3.42 (s, 4H), 2,81 (m, 4H), 1.88 (b, 4H).

3,9-PC2AM^{tBu}: Yield: 0.15 g (70%). $C_{23}H_{40}N_6O_2$ (432.6): calcd. C 63.9, H 9.3, N 19.4; found C 64.0, H 9.2, N 19.5. IR (ATR, cm^{-1}): 1573 (s), 1448 (s) [ν(C=C) and ν(C=N)$_{py}$], 1666 (s) [ν(C=O)], 3282, 3255 (m) [ν(NH)]. MS (ESI-MS, *m/z,* found (calculated)): 433 (433) [**3,9-**PC2AM^{tBu}+H]$^+$. ^{1}H NMR ($CDCl_3$) δ: 7.58 (t, 1H), 7.11 (d, 2H, ^3J = 7.7 Hz), 3.80 (s, 4H), 3.26 (s, 4H), 2.66 (m, 4H), 1.73 (b, 4H), 1.40 (s, 18H).

Preparation of the complexes. General procedure. A solution of $Co(ClO_4)_2{\cdot}6H_2O$ or $Ni(ClO_4)_2{\cdot}6H_2O$ (0.05 mmol) in methanol (5 mL) was added to a stirred solution of 0.05 mmol of **3,9-PC2AM^{H}** or **3,9-PC2AM^{tBu}** in the same solvent (10 mL). Crystalline compounds were obtained for **3,9-PC2AM^{H}** complexes. **3,9-PC2AM^{tBu}** complexes were recrystallized in water with a small amount of KPF_6, yielding the corresponding complexes.

[Ni(3,9-PC2AM^{H})](ClO$_4$)$_2$. Yield: 0.071 g (82%). IR (ATR, cm^{-1}): 1589 (s), 1440 (s) [ν(C=C) and ν(C=N)$_{py}$], 1654 (s) [ν(C=O)], 3293, 3269, 3236 (m) [ν(NH)], 1058 (s) [ν(ClO$_4^-$)]. MS (ESI-MS, *m/z,* found (calculated)): 577.1 (577.0) [Ni(**3,9-PC2AM^{H}**+H)(ClO$_4$)$_2$]$^+$, 477.1 (477.1) [Ni(**3,9-PC2AM^{H}**)(ClO$_4$)]$^+$, 377.1 (377.1) [Ni(**3,9-PC2AM^{H}**-H)]$^+$. $C_{15}H_{24}N_6O_{10}Cl_2Ni$ (577.98): calcd. C 31.2, H 4.2, N 14.5; found C 30.9, H 4.6, N 14.3.

[Co(3,9-PC2AM^{H})](ClO$_4$)$_2$·4.5H$_2$O. Yield: 0.024 g (73%). IR (ATR, cm^{-1}): 1607 (s), 1456 (s) [ν(C=C) and ν(C=N)$_{py}$], 1651 (s) [ν(C=O)], 3286, 3221 (m) [ν(NH)], 1050 (s) [ν(ClO$_4^-$)]. MS (ESI-MS, *m/z,* found (calculated)): 577.1 (577.0) [Co(**3,9-PC2AM^{H}**+H)(ClO$_4$)$_2$]$^+$, 478.1 (478.1) [Co(**3,9-PC2AM^{H}**)(ClO$_4$)]$^+$, 378.1 (378.1) [Co(**3,9-PC2AM^{H}**-H)]$^+$. $C_{15}H_{33}N_6O_{14.5}Cl_2Co$ (659.3): calcd. C 27.3 H 5.0, N 12.7; found C 27.7, H 4.8, N 12.6. A small amount of the solid was dissolved in water and KPF_6 was added, yielding the crystalline complex [Co(**3,9-PC2AM^{H}**)(H$_2$O)](PF$_6$)$_2$·H$_2$O for X-ray diffraction analysis.

[Ni(**3,9-PC2AM^{tBu}**)](PF$_6$)$_2$. Yield: 0.027 g (70%). IR (ATR, cm^{-1}): 1551 (s), 1450 (s) [ν(C=C) and ν(C=N)$_{py}$], 1644 (m), 1622 (m) [ν(C=O)], 3294 (m) [ν(NH)], 823 (s), 553 (s) [ν(PF$_6^-$)]. MS (ESI-MS, *m/z,* found (calculated)): 635.2 (635.2) [Ni(**3,9-PC2AM^{tBu}**)(PF$_6$)]$^+$. $C_{23}H_{40}N_6O_2P_2F_{12}Ni$ (781.23): calcd. C 35.4, H 5.2, N 10.8; found C 35.6, H 5.6, N 10.6.

[Co(**3,9-PC2AM^{tBu}**)](PF$_6$)$_2$·1.875H$_2$O. Yield: 0.029 g (72%). IR (ATR, cm^{-1}): 1577 (m), 1471 (m) [ν(C=C) and ν(C=N)$_{py}$], 1644 (m), 1617 (s) [ν(C=O)], 3331 (m) [ν(NH)], 833 (s), 555 (s) [ν(PF$_6^-$)]. MS (ESI-MS, *m/z,* found (calculated)): 636.2 (636.2) [Co(**3,9-PC2AM^{tBu}**)(PF$_6$)]$^+$. $C_{23}H_{43.75}N_6O_{3.88}P_2F_{12}Co$ (815.26): calcd. C 33.9, H 5.4, N 10.3; found C 33.7, H 5.6, N 10.5.

Sample preparation and potentiometric titrations. Concentration of Co(II) and Ni(II) stock solutions were determined by titrating the metal solutions with standardized Na_2H_2EDTA in urotropine buffer (pH 5.6 – 5.8) in the presence of xylenol orange as an indicator. The $[ML]^{2+}$ complexes were prepared by mixing the ligand and the metal and adjusting the pH to 7.

The concentration of the ligand stock solution was determined by pH-potentiometric titration in the presence and absence of a large (5-fold) excess of $MnCl_2$. The pH-potentiometric titrations were made with standardized 0.16 M NaOH. The protonation constants of the ligands and stability as well as protonation constants of the complexes were determined by pH potentiometric titration with 0.16 M NaOH at 25 °C using a constant ionic strength (0.15 M NaCl) in 6.000 mL samples. The concentration of the ligand and M(II) complexes was generally 0.0025 M. For the pH measurements and titrations, a Metrohm 888 Titrando titration workstation equipped with a Metrohm-6.0234.110 combined electrode was used. The solutions were stirred, and N_2 was bubbled through them. The titrations were made in the pH range of 1.75-11.85. KH-phthalate (pH=4.005) and borax (pH=9.177) buffers were used to calibrate the pH meter. For the calculation of $[H^+]$ from the measured pH values, the method proposed by Irving et al.[68] was used as follows: A 0.012 M HCl solution was titrated with a standardized NaOH solution at 0.15 M NaCl ionic strength. The differences (A) between the measured (pH_{read}) and calculated pH (-log[H$^+$]) value (i.e., the average of A values in the pH-range of 1.75-2.20 was used to obtain the equilibrium H$^+$ concentration from the pH values measured in the titration experiments (A=0.031(2)). For the equilibrium calculations, the stoichiometric water ionic product (pK_w) was also needed to calculate $[OH^-]$ values under basic conditions. The V_{NaOH} – pHr_{ead} data pairs of the HCl – NaOH titration obtained in the pH range 11.20 – 11.85 were used to calculate the pK_w value (pK_w=13.807(8)). The protonation and stability constants were calculated with the PSEQUAD program. Species distribution plots were calculated taking the experimental constants using the computer software HySS.[69]

The protonation constants of the ligand determined by pH-potentiometry are defined by the Equation 8.

$$K_{\mathrm{H}_i\mathrm{L}} = \frac{[\mathrm{H}_i\mathrm{L}]}{[\mathrm{H}^+][\mathrm{H}_{i-1}\mathrm{L}]} \quad (8)$$

where *i*=1 and 2 for the PCTAM^{H} ligand.

Stability constants of complexes and their protonation constants are described and defined in Equations (9) and (10).

$$K_{\mathrm{ML}} = \frac{[\mathrm{ML}]}{[\mathrm{M}][\mathrm{L}]} \quad (9)$$

$$K_{\mathrm{MLH}} = \frac{[\mathrm{MH}_i\mathrm{L}]}{[\mathrm{H}^+][\mathrm{MH}_{i-1}\mathrm{L}]} \quad (8)$$

Where [M], [L], and [ML] are the equilibrium concentrations of free metal ion, deprotonated ligand, and deprotonated complex, respectively.

Kinetic studies. The inertness of the $[Co(PC2AM^{H})]^{2+}$ and $[Ni(PC2AM^{H})]^{2+}$ complexes was characterized by the rates of acid assisted dechelation reactions taking place under acidic conditions. The reactions were studied by spectrophotometry, following the dissociation of the complexes at 230 nm with JASCO V-770 UV-Vis-Nir spectrophotometer. The concentration of the complexes was set to 0.50 mM, while the concentration of the acid was varied in the concentration range of 0.1 – 1.0 M HCl, in order to guarantee pseudo-first-order conditions. The temperature was maintained at 25 °C and the ionic strength of the solutions was kept constant at 1.0 M $(H^+ + Na^+)Cl^-$. The pseudo-first-order rate constants (k_{obs}) were calculated by fitting of the absorbance - time data pairs to eqn. 3 with the Micromath Scientist computer program (version 2.0, Salt Lake City, UT, USA).

CEST measurements. NMR CEST experiments on 20 mM $[Co(3,9\text{-}PC2AM^{H})(H_2O)]^{2+}$ and 15 mM $[Ni(3,9\text{-}PC2AM^{H})]^{2+}$ (pH 7.4, HEPES 50 mM) solutions were performed on a 300 MHz Bruker Avance III NMR spectrometer (Bruker, Ettlingen, Germany). The *z*-spectra were recorded using a saturation time of 2 s at different temperatures (25 and 37 °C for both complexes). For each temperature, data was collected by varying the saturation power (B_1= 2.5, 5, 10, 15, 20, 25 and 30 μT), whilst the saturation time remained constant. The longitudinal and transverse relaxation times, T_1 and T_2, were measured using the inversion-recovery and Carr-Purcell-Meiboom-Gill pulse sequences, respectively. The exchange rates were determined using the qCEST method that is based on the Bloch–McConnell (BM) equations.[70]

Computational details. The positions of H atoms in the X-ray structure of the $[Co(3,9\text{-}PC2AM^{H})(H_2O)]^{2+}$ complex were optimized using spin unrestricted calculations with the hybrid meta-GGA TPSSh exchange correlation functional,[71] the def2-TZVPP basis set[72] and the Gaussian 16 program package (version B.01).[73]

Table 5. Crystal Data and Structure Refinement for $[Ni(\mathbf{3,9\text{-}PC2AM^{H}})](ClO_4)_2$ (Ni-PC2AM^{H}) $[Co(\mathbf{3,9\text{-}PC2AM^{H}})(H_2O)](PF_6)_2\cdot H_2O$ (Co-PC2AM^{H}) $[Ni(\mathbf{3,9\text{-}PC2AM^{tBu}})(H_2O)](PF_6)_2$ (Ni-PC2AM^{tBu}) and $[Co(\mathbf{3,9\text{-}PC2AM^{tBu}})](PF_6)_2$ (Co-PC2AM^{tBu}).

	Ni-PC2AM^{H}	Co-PC2AM^{H}	Ni-PC2AM^{tBu}	Co-PC2AM^{tBu}
formula	$C_{15}H_{24}N_6O_{10}Cl_2Ni$	$C_{15}H_{28}N_6O_4P_2F_{12}Co$	$C_{23}H_{40}N_6O_2P_2F_{12}Ni$	$C_{46}H_{80}N_{12}O_4P_4F_{24}Co_2$
mol wt	578.01	705.30	781.26	1562.96
cryst syst	Triclinic	Monoclinic	Orthorhombic	Monoclinic
space group	P-1	P21/c	Pna21	P21/n
a (Å)	10.2809(6)	10.4836(7)	15.9022(6)	11.7343(11)
b (Å)	10.4879(6)	19.3332(13)	12.0154(4)	33.137(3)
c (Å)	11.4557(7)	13.5320(9)	16.8911(5)	17.0102(17)
α (deg)	66.997(2)			90.496(3)
β deg)	78.831(2)	99.614(2)		
γ (deg)	85.433(2)			
V(Å^3)	1115.45(12)	2704.2(3)	3227.40(19)	6614.0(11)
Z	2	4	4	4
D(calc) (Mg/m^3)	1.721	1.732	1.608	1.570
μ (mm^{-1})	1.176	0.871	0.803	0.716
R_{int}	0.0269	0.0399	0.0310	0.0307
R_1[a]	0.0324	0.0517	0.0242	0.0697
wR_2 (all data)[b]	0.0798	0.1340	0.0568	0.1836

[a] $R1 = \sum ||F_o| - |F_c|| / \sum |F_o|$. [b] $wR2 = \{\sum[w(|F_o|^2 - |F_c|^2)^2]/\sum[w(F_o^4)]\}^{1/2}$.

Calculations of the diamagnetic and paramagnetic shielding constants of $[Co(3,9\text{-}PC2AM^{H})(H_2O)]^{2+}$ were carried out with the ORCA program package (version 4.2.1).[74] Calculations of the hyperfine coupling tensors of ^{1}H nuclei were carried out using the BH&HLYP functional[75] in combination with the def2-TZVPP basis set. The hyperfine coupling constants contain contributions from the isotropic or Fermi contact term, the spin dipolar contribution arising from electron–nuclear dipole–dipole coupling, and the second order contribution from spin-orbit coupling.[76] These calculations were accelerated with the aid of the resolution of identity (RI-JK) approximation,[77] using auxiliary basis sets generated automatically with the Autoaux procedure implemented in ORCA.[78] The integration

grid was augmented from the default values using the grid7 keyword. Spin-orbit coupling was considered using the SOMF(1X) option, which uses the effective potential and mean-field approaches.[79]

Crystal Structure Determinations. Single crystals of [Ni(3,9-PC2AM^{H})]$(ClO_4)_2$, [Co(3,9-PC2AM^{H})(H_2O)]$(PF_6)_2{\cdot}H_2O$, [Ni(3,9-PC2AM^{tBu})(H_2O)]$(PF_6)_2$ and [Co(3,9-PC2AM^{tBu})]$(PF_6)_2$ were obtained and analysed by X-ray diffraction. Table 5 shows selected crystallographic data and structure refinement parameters. Crystallographic data were collected at 100 K using a Bruker D8 Venture diffractometer with a Photon 100 CMOS detector and Mo-Kα radiation (λ = 0.71073 Å) generated by an Incoatec high brillance microfocus source equipped with Incoatec Helios multilayer optics. Frames of data, indexing reflections, and the determination of lattice parameters was collected with APEX3, whilst SAINT[80] and SADABS[81] were used for integration of intensity of reflections, and for scaling and empirical absorption correction respectively. The structure was solved with the program SHELXT.[82] The refining process all non-hydrogen atoms with anisotropic thermal parameters by full-matrix least-squares calculations on F^2, was carried out with SHELXL-2014.[83] Hydrogen atoms were inserted at calculated positions and constrained with isotropic thermal parameters and refined isotropically. Disordered water molecules present were present in the crystal structure of [Co(3,9-PC2AM^{tBu})]$(PF_6)_2$. A solvent masking routine was applied to correct the reflection data for the diffuse scattering associated with them. Molecular graphics were generated using OLEX2.[84] Supplementary crystallographic data are contained in CCDC 2108175 for [Co(**3,9-PC2AM^{H}**)(H_2O)]$(PF_6)_2{\cdot}H_2O$ (Co-PC2AM^{H}), 2108176 for [Ni(**3,9-PC2AM^{H}**)]$(ClO_4)_2$ (Ni-PC2AM^{H}), 2108177 for [Co(**3,9-PC2AM^{tBu}**)]$(PF_6)_2$ (Co-PC2AM^{tBu}) and 2108178 for [Ni(**3,9-PC2AM^{tBu}**)(H_2O)]$(PF_6)_2$ (Ni-PC2AM^{tBu}). These data can be obtained free of charge via www.ccdc.cam.ac.uk/data_request/cif, or by emailing data_request@ccdc.cam.ac.uk, or by contacting The Cambridge Crystallographic Data Centre, 12 Union Road, Cambridge CB2 1EZ, UK; fax: + 44 1223 336033.

Conflicts of interest

There are no conflicts to declare.

Acknowledgements

The authors acknowledge the Spanish Ministerio de Economía y Competitividad (grant CTQ2016-76756-P) and Xunta de Galicia (ED431B 2020/52) for generous financial support. C. P.-I. and D. E.-G. thank Centro de Supercomputación de Galicia (CESGA) for providing the supercomputing facilities. P. P.-L. and L. V. are in debt with CACTI (Universidade de Vigo) for X-ray measurements. E.M., F.A. and G.T. are grateful to the Hungarian National Research, Development and Innovation Office (Projects NKFIH K-120224 and 134694) for their financial support. E.M. was also supported by the Doctoral School of Chemistry at the University of Debrecen, Debrecen, Hungary. G. A. is thankful for the financial support from the Shanghai Municipal Science and Technology Major Project (Grant No. 2019SHZDZX02). G.T. and C.P.-I. gratefully acknowledge the COST Action CA15209 "European Network on NMR Relaxometry" and the bilateral Hungarian−Spanish Science and Technology Cooperation Program (2019-2.1.11- TET-2019-00084 supported by NKFIH).

References

1 B. Wu, G. Warnock, M. Zaiss, C. Lin, M. Chen, Z. Zhou, L. Mu, D. Nanz, R. Tuura and G. Delso, *EJNMMI Phys.,* 2016, **3**, 19 ; (b) M. Zaiss and P. Bachert, *Phys. Med. Biol.,* 2013, **58**, R221-R269.

2 (a) P. C. M. van Zijl and N. N. Yadav, *Magn. Reson. Med.,* 2011, **65**, 927-948 ; (b) E. Terreno, D. Delli Castelli and S. Aime, *Contrast Media Mol. Imaging,* 2010, **5**, 78–98

3 S. D. Wolff and R. S. Balaban, *Magn. Reson.Med.,* 1989, **10**, 135-144.

4 K. M. Ward, A. H. Aletras and R. S. Balaban. *J. Magn. Reson.,* 2000, **143**, 79–87.

5 S. Zhang, P. Winter, K. Wu and A. D. Sherry, *J. Am. Chem. Soc.,* 2001, **123**, 1517-1518.

6 S. Aime, A. Barge, D. Delli Castelli, F. Fedeli, A. Mortillaro, F. U. Nielsen and E. Terreno, *Magn. Reson. Med.,* 2002, **47**, 639-648.

7 (a) M. Woods, D. E. Woessner and A. D. Sherry, *Chem. Soc. Rev.,* 2006, **35**, 500–511 ; (b) S. Zhang, M. Merritt, D. E. Woessner, R. E. Lenkinski and A. D. Sherry, *Acc. Chem. Res.,* 2003, **36**, 783-790 ; (c) S. Viswanathan, Z. Kovacs, K. N. Green, S. J. Ratnakar and A. D. Sherry, *Chem. Rev.,* 2010, **110**, 2960-3018.

8 E. Terreno, D. Delli Castelli, A. Vialle and S. Aime, *Chem. Rev.,* 2010, **110**, 3019-3042.

9 A. Rodríguez-Rodríguez, M. Zaiss, D. Esteban-Gómez, G. Angelovski and C. Platas-Iglesias, *Int. Rev. Phys. Chem.,* 2021, **40**, 51-79.

10 J. A. Peters, J. Huskens and D. J. Raber, *Prog. Nucl. Magn. Reson. Spectrosc.,* 1996, **28**, 283-350.

11 J. Kim, Y. Wu, Y. Guo, H. Zheng and P. Z. Sun, *Contrast Media Mol. Imaging*, 2015, **10**, 163–178.

12 X. Wang, Y. Wu, T. C. Soesbe, J. Yu, P. Zhao, G. E. Kiefer and A. D. Sherry, Angew. Chem. Int. Ed., 2015, **54**, 8662 –8664.

13 (a) D. Castelli, G. Ferrauto, J. C. Cutrin, E. Terreno and S. Aime, *Magn. Reson. Med.* 2014, **71**, 326–332 ; (b) Y. Li, V. R. Sheth, G. Liu and M. D. Pagel, *Contrast Media Mol. Imaging,* 2011, **6**, 219–228 ; (c) D. V. Hingorani, A. S. Bernstein and M. D. Pagel, *Contrast Media Mol. Imaging,* 2015, **10**, 245–265.

14 S. J. Dorazio, P. B. Tsitovich, K. E. Siters, J. A. Spernyak and J. R. Morrow, *J. Am. Chem. Soc.,* 2011, **133**, 14154-14156.

15 S. J. Dorazio, A. O. Olatunde, J. A. Spernyak and J. R. Morrow, *Chem. Commun.,* 2013, **49**, 10025-10027.

16 A. O. Olatunde, S. J. Dorazio, J. A. Spernyak, J. R. Morrow, *J. Am. Chem. Soc.,* 2012, **134**, 18503-18505.

17 K. Du and T. D. Harris, *J. Am. Chem. Soc.,* 2016, **138**, 7804-7807.

18 A. Gupta, P. Caravan, W. S. Price, C. Platas-Iglesias, E. M. Gale, *Inorg. Chem.,* 2020, *59*, 6648−6678.

19 S. M. Pinto, V. Tomé, M. J.F. Calvete, M. M. C.A. Castro, É. Tóth and C. F. G. C. Geraldes, *Coord. Chem. Rev.,* 2019, **390**, 1–31.

20 (a) S. J. Dorazio, P. B. Tsitovich, S. A. Gardina and J. R. Morrow, *J. Inorg. Biochem.*, 2012, **117**, 212-219 ; (b) P. B. Tsitovich, P. J. Burns, A. M. McKay and J. R. Morrow, *J. Inorg. Biochem.*, 2014, **133**, 143-154.

21 (a) S. J. Dorazio and J. R. Morrow, *Inorg. Chem.,* 2012, **51**, 7448−7450 ; (b) S. M. Abozeid, E. M. Snyder, T. Y. Tittiris, C. M.

Steuerwald, A. Y. Nazarenko and J. R. Morrow, *Inorg. Chem.,* 2018, **57**, 2085−2095.
22 (a) P. J. Burns, J. M. Cox and J. R. Morrow, *Inorg. Chem.,* 2017, **56**, 4545−4554; (b) P. B. Tsitovich, J. A. Spernyak and J. R. Morrow, *Angew. Chem. Int. Ed.,* 2013, **52**, 13997 –14000.
23 A. Rodríguez-Rodríguez, M. Zaiss, D. Esteban-Gómez, G. Angelovski and C. Platas-Iglesias, *Met. Ions Life Sci.,* 2021, in press.
24 L. Caneda-Martínez, L. Valencia, I. Fernández-Pérez, M. Regueiro-Figueroa, G. Angelovski, I. Brandariz, D. Esteban-Gómez and C. Platas-Iglesias, *Dalton Trans.,* 2017, *46*, 15095.
25 C. J. Bond, R. Cineus, A. Y. Nazarenko, J. A. Spernyak and J. R. Morrow, *Dalton Trans.,* 2020, **49**, 279–284.
26 M. Yu, B. S. Bouley, D. Xie and E. L. Que, *Dalton Trans.,* 2019, **48**, 9337–9341.
27 (a) A. O. Olatunde, C. J. Bond, S. J. Dorazio, J. M. Cox, J. B. Benedict, M. D. Daddario, J. A. Spernyak and J. R. Morrow, *Chem. Eur. J.,* 2015, **21**, 18290 – 18300 ; (b) P. B. Tsitovich, J. M. Cox, J. A. Spernyak and J. R. Morrow, *Inorg. Chem.,* 2016, **55**, 12001−12010.
28 S. J. Dorazio, A. O. Olatunde, P. B. Tsitovich and J. R. Morrow, *J. Biol. Inorg. Chem.,* 2014, **19**, 191–205.
29 R. N. Pradhan, S. Chakraborty, P. Bharti, J. Kumar, A. Ghosh and A. K. Singh, *Dalton Trans.,* 2019, **48**, 8899–8910.
30 Z. Garda, E. Molnár, N. Hamon, J. L. Barriada, D. Esteban-Gómez, B. Váradi, V. Nagy, K. Pota, F. K. Kálmán, I. Tóth, N. Lihi, C. Platas-Iglesias, É. Tóth, R. Tripier and G. Tircsó, *Inorg. Chem.,* 2021, 60, 1133-1148.
31 B. Drahos, J. Kotek, I. Cisarova, P. Hermann, L. Helm, I. Lukes, and E. Toth, *Inorg. Chem.,* 2011, **50**, 12785-12801.
32 G. Bao, S. Zha, Z. Liu, Y.-H. Fung, C.-F. Chan, H. Li, P.-H. Chu, D. Jin**,** P. A. Tanner and K.-L. Wong *Inorg. Chem*., 2018, **57**, 120-128.
33 D. Casanova, P. Alemany, J. M. Bofill and S. Alvarez, *Chem. Eur. J.,* 2003, **9**, 1281-1295.
34 C. Platas-Iglesias, L. Vaiana, D. Esteban-Gómez, F. Avecilla, J. A. Real, A. de Blas and T. Rodríguez-Blas, *Inorg. Chem.,* 2005, **44**, 9704-9713.
35 B. Drahoš, I. Císařová, O. Laguta, V. T. Santana, P. Neugebauer, and R. Herchel, *Dalton Trans.,* 2020, **49**, 4425–4440.
36 J. Dale, *Acta Chem. Scand.,* 1973, **27**, 1115-1129.
37 G. E. Kiefer and M. Woods*, Inorg. Chem.,* 2009, **48**, 11767–11778.
38 (a) M. P. Clares, S. Blasco, M. Inclán, L. del Castillo Agudo, B. Verdejo, C. Soriano, A. Doménech, J. Latorre, E. Garcia-España, *Chem. Commun.,* 2011, **47**, 5988−5990. (b) J.-H. Wen, C.-Y. Li, Z.-R. Geng, X.-Y. Ma, Z.-L. Wang, *Chem. Commun.,* 2011, **47**, 11330−11332.
39 J. K. Beattie, *Acc. Chem. Res.,* 1971, **4**, 253-259.
40 S. Aime, M. Botta, S. Geninatti Crich, G. B. Giovenzana, G. Jommi, R. Pagliarin and M. Sisti, *Inorg. Chem.* 1997, *36*, 2992–3000.
41 Z. Garda, A. Forgács, Q. N. Do, F. K. Kálmán, S. Timári, Z. Baranyai, L. Tei, I. Tóth, Z. Kovács and G. Tircsó, *J. Inorg. Biochem.* 2016, **163**, 206–213.
42 A. Forgács, L. Tei, Z. Baranyai, I. Tóth, L. Zékány and M. Botta, *Eur. J. Inorg. Chem.,* 2016, 1165–1174.
43 (a) M. R. S. Amorim, R. Delgado and J. J. R. F. Da Silva, *Polyhedron*, 1992, **11**, 1891-1899 ; (b) F. K. Kálmán 1, V. Nagy, R. Uzal-Varela, P. Pérez-Lourido, D. Esteban-Gómez, Z. Garda, K. Pota, R. Mezei, A. Pallier, É. Tóth, C. Platas-Iglesias and G. Tircsó, *Molecules,* 2021, **26**, 1524
44 Z. Garda, E. Molnár, F. K. Kálmán, R. Botár, V. Nagy, Z. Baranyai, E. Brücher, Z. Kovács, I. Tóth and G. Tircsó, Front. Chem., 2018, 6, 232.
45 A. Jancso, K. Selmeczi, P. Gizzi, N. V. Nagy, T. Gajda and B. Henry, *J. Inorg. Biochem.,* 2011, **105**, 92.
46 J. M. Weeks, M. R. Taylor and K. P. Wainwright, *J. Chem. Soc., Dalton Trans.,* 1997, 317–322.
47 H. Irving and R. J. P. Williams, *J. Chem. Soc.,* 1953, 3192-3210.
48 C. J. Bond, G. E. Sokolow, M. R. Crawley, P. J. Burns, J. M. Cox, R. Mayilmurugan and J. R. Morrow, *Inorg. Chem.,* 2019, **58**, 13, 8710–8719.
49 L. Vaiana, M. Regueiro-Figueroa, M. Mato-Iglesias, C. Platas-Iglesias, D. Esteban-Gómez, A. de Blas and T. Rodríguez-Blas, *Inorg. Chem.,* 2007, **46**, 8271-8282.
50 M. Regueiro-Figueroa, L. M. P. Lima, V. Blanco, D. Esteban-Gómez, A. de Blas, T. Rodríguez-Blas, R. Delgado and C. Platas-Iglesias, *Inorg. Chem.,* 2014, **53**, 12859−12869.
51 (a) Z. Baranyai, Z. Pálinkás, F. Uggeri, A. Maiocchi, S. Aime and E. Brücher, *Chem. Eur. J.,* 2012, **18**, 16426–16435; (b) L. Sarka, L. Burai and E. Brücher, *Chem. Eur. J.,* 2000, **6**, 719–724 ; (c) Z. Baranyai, E. Brücher, F. Uggeri, A. Maiocchi, I. Tóth, M. Andrási, A. Gáspár, L. Zékány and S. Aime, *Chem. Eur. J.,* 2015, **21**, 4789 – 4799.
52 Z. Jászberényi, É. Tóth, T. Kálai, R. Király, L. Burai, E. Brücher, A. E. Merbach and K. Hideg, *Dalton Trans.,* 2005, 694.
53 D. Ndiaye, M. Sy, A. Pallier, S. Même, I. de Silva, S. Lacerda, A. M. Nonat, L. J. Charbonnière and Éva Tóth, *Angew. Chem. Int. Ed.,* 2020, **59**, 11958.
54 E. Brücher, G. Tircsó, Z. Baranyai, Z. Kovács and A. D. Sherry, in The Chemistry of contrast agents in medical magnetic resonance imaging, Stability and Toxicity of Contrast Agents, 2nd Ed., Eds. A. Merbach, L. Helm and E. Tóth (Chichester: John Wiley and Sons), 157–208.
55 K. Długopolska, J. Kisała, M. Danilczuk, D. Pogocki and T. Ruman, *Appl. Magn. Reson.* 2010, **38**, 321–335.
56 J. Blahut, L. Benda, J. Kotek, G. Pintacuda and P. Hermann, *Inorg. Chem.,* 2020, **59**, 10071−10082.
57 (a) A. A. Pavlov, S. A. Savkina, A. S. Belov, Y. Z. Voloshin, Y. V. Nelyubina and V. V. Novikov, *ACS Omega*, 2018, **3**, 4941−4946 ; (b) A. S. Belov, Y. Z. Voloshin, A. A. Pavlov, Y. V. Nelyubina, S. A. Belova, Y. V. Zubavichus, V. V. Avdeeva, N. N. Efimov, E. A. Malinina, K. Y. Zhizhin and N. T. Kuznetsov, *Inorg. Chem.,* 2020, **59**, 5845−5853 ; (c) J. Mares and J. Vaara *Phys. Chem. Chem. Phys.,* 2018, **20**, 22547—22555 ; (d) Q. Miao, W.-M. Liu, T. Kock, A. Blok, M. Timmer, M. Overhand and M. Ubbink, *Angew. Chem. Int. Ed.,* 2019, **58**, 13093–13100.
58 L. Lang, E. Ravera, G. Parigi, C. Luchinat and F. Neese, *J. Phys. Chem. Lett.,* 2020, **11**, 8735−8744.
59 (a) A. Soncini and W. Van den Heuvel, *J. Chem. Phys.,* 2013, **138**, 021103 ; (b) W. Van den Heuvel and A. Soncini, *J. Chem. Phys.,* 2013, **138**, 054113.
60 J. H. Forsberg, R. M. Delaney, Q. Zhao, G. Harakas and R. Chandran, *Inorg. Chem.,* **1995**, *34*, 3705-3715.
61 I. Bertini, C. Luchinat and G. Parigi, *Prog. Nucl. Magn. Reson. Spectrosc.,* 2002, **40**, 249-273.
62 G. Castro, M. Regueiro-Figueroa, D. Esteban-Gómez, P. Pérez-Lourido, C. Platas-Iglesias and L. Valencia, *Inorg. Chem.,* 2016, **55**, 3490−3497
63 T. Gambino, L. Valencia, P. Pérez-Lourido, D. Esteban-Gómez, M. Zaiss, C. Platas-Iglesias and G. Angelovski, *Inorg Chem. Front.*, 2020, **7**, 2274–2286.
64 A. Rodríguez-Rodríguez, M. Zaiss, D. Esteban-Gómez, G. Angelovski and C. Platas-Iglesias, Metal Ion Complexes in Paramagnetic Chemical Exchange Saturation Transfer (ParaCEST): Metal Ions in Bio-Imaging Techniques, edited by Astrid Sigel, Eva Freisinger and Roland K.O. Sigel, Berlin, Boston: De Gruyter, 2021, pp. 101-136.

65 R. Pujales-Paradela, T. Savic, I. Brandariz, P. Pérez-Lourido, G. Angelovski, D. Esteban-Gómez and C. Platas-Iglesias, *Chem. Commun.,* 2019, **55**, 4115—4118.

66 J. M. Siaugue, F. Segat-Dioury, I. Sylvestre, A. Favre-Reguillon, J. Foos, C. Madic and A. Guy, *Tetrahedron*, 2001, **57**, 4713–4718.

67 D. S. S. M. Uppu, M. Bhowmik, S. Samaddar, J. Haldar, *Chem. Commun*., 2016, **52**, 4644-4647.

68 H. M. Irving, M. G. Miles and L. D. Pettit, *Anal. Chim. Acta,* 1967, **38**, 475−488.

69 L. Alderighi, P. Gans, A. Ienco, D. Peters, A. Sabatini and A. Vacca, *Coord. Chem. Rev*. 1999, **184**, 311.

70 M. Zaiss, G. Angelovski, E. Demetriou, M. T. McMahon, X. Golay, and K. Scheffler, *Magn. Reson. Med.,* 2018, **79**, 1708–1721.

71 J. M. Tao, J. P. Perdew, V. N. Staroverov and G. E. Scuseria, *Phys. Rev. Lett.,* 2003, **91**, 146401.

72 F. Weigend and R. Ahlrichs, *Phys. Chem. Chem. Phys.,* 2005, **7**, 3297.

73 Gaussian 16, Revision B.01, M. J. Frisch, G. W. Trucks, H. B. Schlegel, G. E. Scuseria, M. A. Robb, J. R. Cheeseman, G. Scalmani, V. Barone, G. A. Petersson, H. Nakatsuji, X. Li, M. Caricato, A. V. Marenich, J. Bloino, B. G. Janesko, R. Gomperts, B. Mennucci, H. P. Hratchian, J. V. Ortiz, A. F. Izmaylov, J. L. Sonnenberg, D. Williams-Young, F. Ding, F. Lipparini, F. Egidi, J. Goings, B. Peng, A. Petrone, T. Henderson, D. Ranasinghe, V. G. Zakrzewski, J. Gao, N. Rega, G. Zheng, W. Liang, M. Hada, M. Ehara, K. Toyota, R. Fukuda, J. Hasegawa, M. Ishida, T. Nakajima, Y. Honda, O. Kitao, H. Nakai, T. Vreven, K. Throssell, J. A. Montgomery, Jr., J. E. Peralta, F. Ogliaro, M. J. Bearpark, J. J. Heyd, E. N. Brothers, K. N. Kudin, V. N. Staroverov, T. A. Keith, R. Kobayashi, J. Normand, K. Raghavachari, A. P. Rendell, J. C. Burant, S. S. Iyengar, J. Tomasi, M. Cossi, J. M. Millam, M. Klene, C. Adamo, R. Cammi, J. W. Ochterski, R. L. Martin, K. Morokuma, O. Farkas, J. B. Foresman, and D. J. Fox, Gaussian, Inc., Wallingford CT, 2016.

74 (a) F. Neese, The ORCA program system. *Wiley Interdiscip. Rev.: Comput. Mol. Sci.,* 2012, *2*, 73−78 ; (b) F. Neese, *Wiley Interdiscip. Rev.: Comput. Mol. Sci.,* 2018, **8**, e1327.

75 A. D. Becke *J. Chem. Phys.,* 1993, **98**, 1372–1377.

76 F. Neese, *Coord. Chem. Rev.,* 2009, **253**, 526-563.

77 (a) F. Weigend, M. Kattanneck and R. Ahlrich, J. Chem. Phys., 2009, **130**, 164106 ; (b) S. Kossmann and F. Neese, *Chem. Phys. Lett.,* 2009, **481**, 240–243.

78 G. L. Stoychev, A. A. Auer and F. Neese, *J. Chem. Theory Comput.,* 2017, **13**, 554-562.

79 F. Neese, *J. Chem. Phys.,* 2005, **122**, 034107.

80 APEX3 and SAINT; Bruker AXS Inc.: Madison, WI, 2016. 1132.

81 Sheldrick, G. M. SADABS, Program for Empirical Absoption Correction of Area Detector Data; University of Göttingen: Göttingen, 1134 Germany, 1996.

82 Sheldrick, G. M. SHELXT − Integrated space-group and crystal-structure determination. Acta Crystallogr., Sect. A: Found. Adv. 2015, A71, 3−8.

83 Sheldrick, G.M. Crystal Structure Refinement with SHELXL. Acta Crystallographica Sect. C, 2015, C71, 3-8.

84 Dolomanov, O. V.; Bourhis, L. J.; Gildea, R. J.; Howard, J. A. K.; Puschmann, H. OLEX: A Complete Structure Solution, Refinement and Analysis Program. J. Appl. Crystallogr. 2009, 42, 339−341.